nature cell biology

Fibroblast polarization is a matrix-rigidity-dependent process controlled by focal adhesion mechanosensing

Masha Prager-Khoutorsky[1,4,5], Alexandra Lichtenstein[1,4], Ramaswamy Krishnan[2,5], Kavitha Rajendran[2,5], Avi Mayo[1], Zvi Kam[1], Benjamin Geiger[1,6] and Alexander D. Bershadsky[1,3,6]

Cell elongation and polarization are basic morphogenetic responses to extracellular matrix adhesion. We demonstrate here that human cultured fibroblasts readily polarize when plated on rigid, but not on compliant, substrates. On rigid surfaces, large and uniformly oriented focal adhesions are formed, whereas cells plated on compliant substrates form numerous small and radially oriented adhesions. Live-cell monitoring showed that focal adhesion alignment precedes the overall elongation of the cell, indicating that focal adhesion orientation may direct cell polarization. siRNA-mediated knockdown of 85 human protein tyrosine kinases (PTKs) induced distinct alterations in the cell polarization response, as well as diverse changes in cell traction force generation and focal adhesion formation. Remarkably, changes in rigidity-dependent traction force development, or focal adhesion mechanosensing, were consistently accompanied by abnormalities in the cell polarization response. We propose that the different stages of cell polarization are regulated by multiple, PTK-dependent molecular checkpoints that jointly control cell contractility and focal-adhesion-mediated mechanosensing.

Cells adhering to the extracellular matrix can sense and respond to a wide variety of chemical and physical features of the adhesive surface, including the molecular nature of the adhesive ligands and their local densities, as well as surface topography and rigidity[1–3]. Rigidity sensing (the capacity to differentially respond to substrates with varying degrees of stiffness) is a general phenomenon affecting multiple cellular properties, including morphology, migratory capacity, gene expression profile and, eventually, cell differentiation and fate[4–6].

Here, we focus on the role of rigidity sensing in regulating the polarization of cultured fibroblasts, and search for the molecules involved in this process. It has been extensively documented that cells acquire anterior–posterior polarity in response to anisotropy of the extracellular environment, both *in vivo* and in culture, as well as undergo spontaneous polarization in an isotropic environment, such as a uniform rigid substrate[7,8].

To gain insights into the role of extracellular matrix rigidity in the polarization of adherent fibroblasts, we used a short interfering RNA (siRNA)-mediated knockdown approach to perturb a central signalling system; namely, PTKs in cultured human fibroblasts[9], plated on matrices of varying rigidities. In so doing, we demonstrated that cell polarization, manifested by cytoskeletal alignment, cell elongation and the development of long stable edges, indeed depends on matrix rigidity. Monitoring of this process indicated that cell elongation is preceded by the alignment of focal adhesions. siRNA-mediated knockdown of 85 PTKs highlighted several molecules whose suppression affects the range of the cell rigidity response, including differential traction force generation and focal adhesion assembly on the substrates with varying rigidities, as well as the extent of rigidity-dependent polarization. These findings imply that the range of rigidities to which cells respond is tunable, and that PTKs play a central role in regulating this process at several levels, including traction force generation, focal adhesion alignment and whole-cell elongation.

RESULTS

Fibroblast polarization is dependent on substrate stiffness

The spreading of cultured fibroblasts on rigid surfaces proceeds in two distinct stages: radial spreading, followed by cell polarization[7]. The polarization step is characterized by an increase in the cell's aspect ratio, the formation of long actomyosin bundles (stress fibres) running along the major cell axis and the development of stable cell edges (see definitions in Supplementary Fig. S1a). To determine the effect of matrix rigidity on this process, we plated human foreskin fibroblasts (HFFs) on two elastomeric systems: poly(dimethylsiloxane) (PDMS) and polyacrylamide (PAA) gels, with rigidities ranging

[1]Department of Molecular Cell Biology, Weizmann Institute of Science, Rehovot 76100, Israel. [2]Department of Environmental Health, Harvard School of Public Health, Boston, Massachusetts 02115, USA. [3]Mechanobiology Institute, National University of Singapore, 117411, Singapore. [4]These authors contributed equally to this work. [5]Present addresses: Centre for Research in Neuroscience, McGill University, Montreal QC, H3G1A4, Canada (M.P-K.); Center for Vascular Biology Research, Beth Israel Deaconess Medical Center and Harvard Medical School, Boston, Massachusetts 02215, USA (R.K., K.R.).
[6]Correspondence should be addressed to B.G. or A.D.B. (e-mail: benny.geiger@weizmann.ac.il or alexander.bershadsky@weizmann.ac.il)

Received 18 August 2011; accepted 27 September 2011; published online 13 November 2011; DOI: 10.1038/ncb2370

from 4 kPa to 2 MPa. Both types of substrate were coated with the matrix protein fibronectin.

Examination of the images of actin-stained cells indicated that cells cultured on glass or elastomeric substrates with a Young's modulus from 150 kPa to 2 MPa were highly polarized. A substantial degree of polarization was also observed on substrates with a Young's modulus of around 30 kPa, whereas cells plated on PDMS or PAA gels with a Young's modulus of about 5 kPa remained largely radial, with less prominent, mostly peripheral, actin bundles (Fig. 1a,b). On the basis of these observations, we selected for further study a pair of fibronectin-coated PDMS substrates with Young's moduli of 2 MPa and 5 kPa, respectively, as our standard 'rigid' (stiff) and 'compliant' (soft) substrates.

Examining the time course of polarization (Fig. 1c) indicated that cell elongation on rigid substrates markedly increased from 2 to 4 h after seeding, and reached a plateau at around 4 to 6 h. During that same time period, cell elongation on the compliant substrate increased very slowly, if at all. Moreover, other manifestations of cell polarity (namely, the formation of long stress fibres along the major cell axis and development of long stable edges) were similarly affected by matrix rigidity. Typical examples of cell polarization and spreading on rigid and compliant PDMS are shown in Supplementary Movie S1.

In a series of control experiments, we demonstrated that fibroblasts polarize properly on rigid, fibronectin- but not poly-L-lysine-coated substrates, supporting the important role of integrin-mediated adhesion in this process. Moreover, myosin-II-driven contractility and intact microtubules were also required for proper rigidity-dependent cell polarization (Supplementary Fig. S1b,c).

Focal adhesion morphology and dynamics depend on substrate stiffness

Examination of focal adhesion formation on rigid and compliant substrates, using HFFs expressing paxillin–YFP, showed major differences in focal adhesion morphology and dynamics. Already within 1 h of plating, focal adhesions formed on the rigid PDMS were about twofold larger than those formed on the compliant surface, even though the aspect ratio of the focal adhesions on both substrates was still low at that time (Fig. 2a,b). Within 6 h, focal adhesions in cells plated on the rigid substrate became less numerous, elongated and oriented themselves along the major cell axis, co-aligned with stress fibres (Fig. 2a,b). On the compliant PDMS, cells formed more numerous but small, radially oriented focal adhesions with low aspect ratios, even 6 h after plating (Fig. 2a,b). Matrix rigidity had no significant effect on the total focal adhesion area of HFF cells (the average area of a single focal adhesion multiplied by the average number of focal adhesions per cell; Supplementary Fig. S3), nor on the mean intensity of the paxillin–YFP fluorescence signal per cell (Fig. 2b).

Comparison of focal adhesion characteristics 6 h after plating showed a positive correlation of focal adhesion area, aspect ratio and orientation with cell aspect ratio, and a negative correlation between cell aspect ratio and the number of focal adhesions per cell (Fig. 2c).

Assessment of focal adhesion dynamics on stiff and compliant substrates by means of live-cell video microscopy was then undertaken, to measure the degree of overlap between focal adhesion images at different times (Supplementary Fig. S2 and Movie S2). This analysis indicated that focal adhesions on the rigid substrate are, on average, considerably less dynamic than those formed on the compliant substrate.

Focal adhesion alignment tends to precede cell elongation

A closer look at the scattergrams in Fig. 2c revealed that many cells on the rigid substrate that had low aspect ratios, nevertheless contained elongated and uniformly oriented focal adhesions. This observation raised the possibility that focal adhesion alignment may precede cell elongation, and determine the direction of the future elongation axis. To that end, we analysed several movies of cell spreading in which focal adhesions were visualized by means of a paxillin–YFP fluorescence signal. In agreement with previous studies[7], we found that in all cases, cells first spread isotropically, acquiring a radially symmetrical, discoid shape before undergoing polarization (usually within 2–6 h after plating). The mode of symmetry breaking was, however, quite diverse: some cells extended a large protrusion while the bulk of the focal adhesions were still radially oriented, and then elongated in the direction of that protrusion (13 out of 43 sequences analysed); whereas other cells retracted part of their leading edge[10], acquiring a crescent-shaped morphology with a non-attached ('stable') edge, along which the cell then elongated (16 out of 43 sequences). Remarkably, however, a significant fraction of cells (14 out of 43 sequences) were characterized by the apparent alignment of focal adhesions in the direction of the future major axis of cell elongation, even while the cells were still rather disc-shaped (Fig. 2d,e, and Supplementary Movie S3). The graphs in Fig. 2e show that during cell spreading, an increase in the focal adhesion orientation (FAO) index precedes the increase in cell aspect ratio. Thus, focal adhesion co-alignment can develop independently of and precede cell elongation.

siRNA-mediated knockdown of specific PTK genes affects rigidity-dependent cell polarization

To explore the molecular mechanisms underlying rigidity-dependent cell polarization, we screened for siRNA-mediated modulation of cell polarization on rigid and compliant substrates. We targeted human PTKs, in view of the central involvement of these signalling molecules in focal adhesion formation[11,12], as well as in the cell's response to substrate rigidity[12,13].

To select the candidate genes, we measured parameters characterizing cell polarization (Supplementary Fig. S1a), as well as projected cell area for each of the knocked-down cell types growing on either rigid or compliant substrates. We based our selection of candidate genes on their effects on differential cell elongation (cell aspect ratio) on rigid and compliant substrates (Supplementary Table S1). On the basis of the nature of the effects of the different siRNAs, they were divided into three main groups (Table 1 and Supplementary Table S1).

The first group of PTK candidates (CSF1R, CSK, FER, ERBB4 and FLT3) comprised genes whose knockdown resulted in a lack of cell elongation on both types of substrate. Knockdown of the second group (AXL, ROR2, JAK1, ERBB3, PTK9, FGFR4, FLT4, LTK, KDR, TYRO3 and DDR2) had the opposite effect; namely, cells demonstrated elongation on both rigid and compliant surfaces. The third group of candidates (NTRK2, NTRK3, MET and PTK2B) comprised genes whose knockdown led to an increase in the cells' ability to differentially respond to the rigid and compliant substrates, compared with control cells. Typical morphologies seen

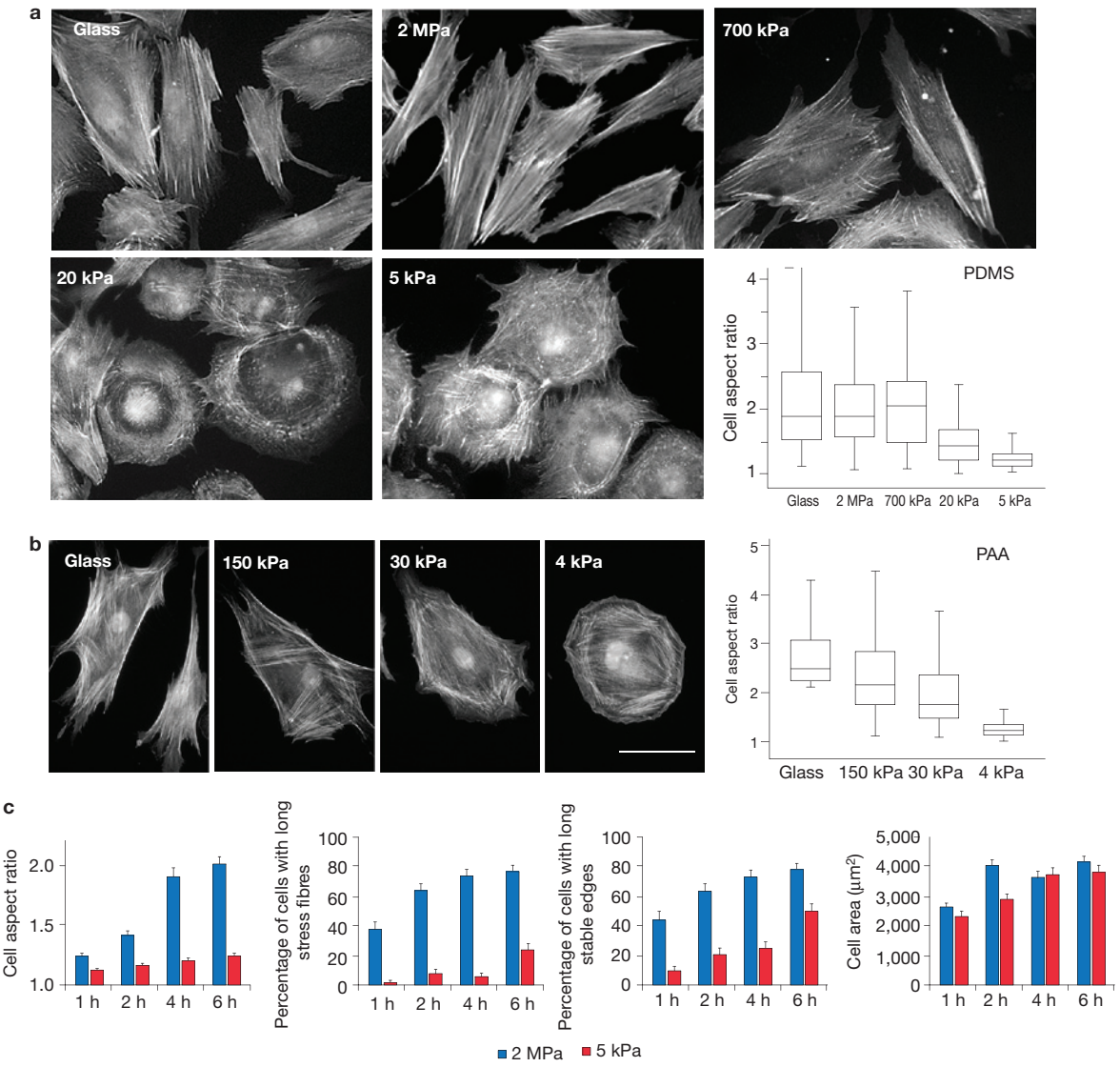

Figure 1 Fibroblasts polarize on rigid, but not on compliant, substrates. (**a**,**b**) The images show HFF cells plated on fibronectin-coated glass or substrates of varying rigidities made of PDMS (**a**) or PAA (**b**) fixed 6 h after plating and stained with TRITC–phalloidin. Scale bar, 40 μm. The corresponding graphs show the values of cell aspect ratio. The aspect ratio values are presented as box-and-whisker plots[28]. At least 100 cells were measured on the substrate of each type in **a** and at least 50 cells in **b**. (**c**) Graphs showing the changes, over time, in parameters characterizing cell polarity, in cells spreading on rigid (2 MPa) and compliant (5 kPa) substrates. HFF cells were plated on fibronectin-coated PDMS substrates, and fixed at different times. From left to right: cell aspect ratio, percentage of cells with long stress fibres, percentage of cells with long stable edges, and cell projected area. All parameters were determined for at least 100 cells for each time point. Error bars represent the s.e.m. Dynamics of cell spreading on rigid and compliant substrates are shown in Supplementary Movie S1.

in members of each group are shown in Fig. 3a. Notably, we found no apparent correlation between the ability of cells to polarize, and their projected area on either substrate (Table 1 and Supplementary Table S1d).

To assess the reliability of the knockdown results, and exclude off-target effects, validation of the knockdown candidates was carried out using individual siRNA sequences corresponding to those in the same Dharmacon SMARTpool used for the screening (Supplementary Table S2). Candidates that did not pass validation were FLT3 and NTRK2.

To further characterize the phenotypes of selected knockdown cells with abnormal polarization behaviour, we carried out measurements of focal adhesions and traction forces developed by these cells on the substrates with different rigidities. Typical examples of the focal adhesions and traction maps for the members of each group of knockdowns are shown in Fig. 3. Alterations in focal adhesion parameters and traction forces caused by all selected knockdowns are characterized and analysed in the following section.

Differential response of focal adhesions and cell traction forces to substrate rigidity in PTK-knockdown cells with altered rigidity-dependent polarization

We first considered the overall features of focal adhesions (FAO, as well as their number and total area per cell). In those knockdown cells

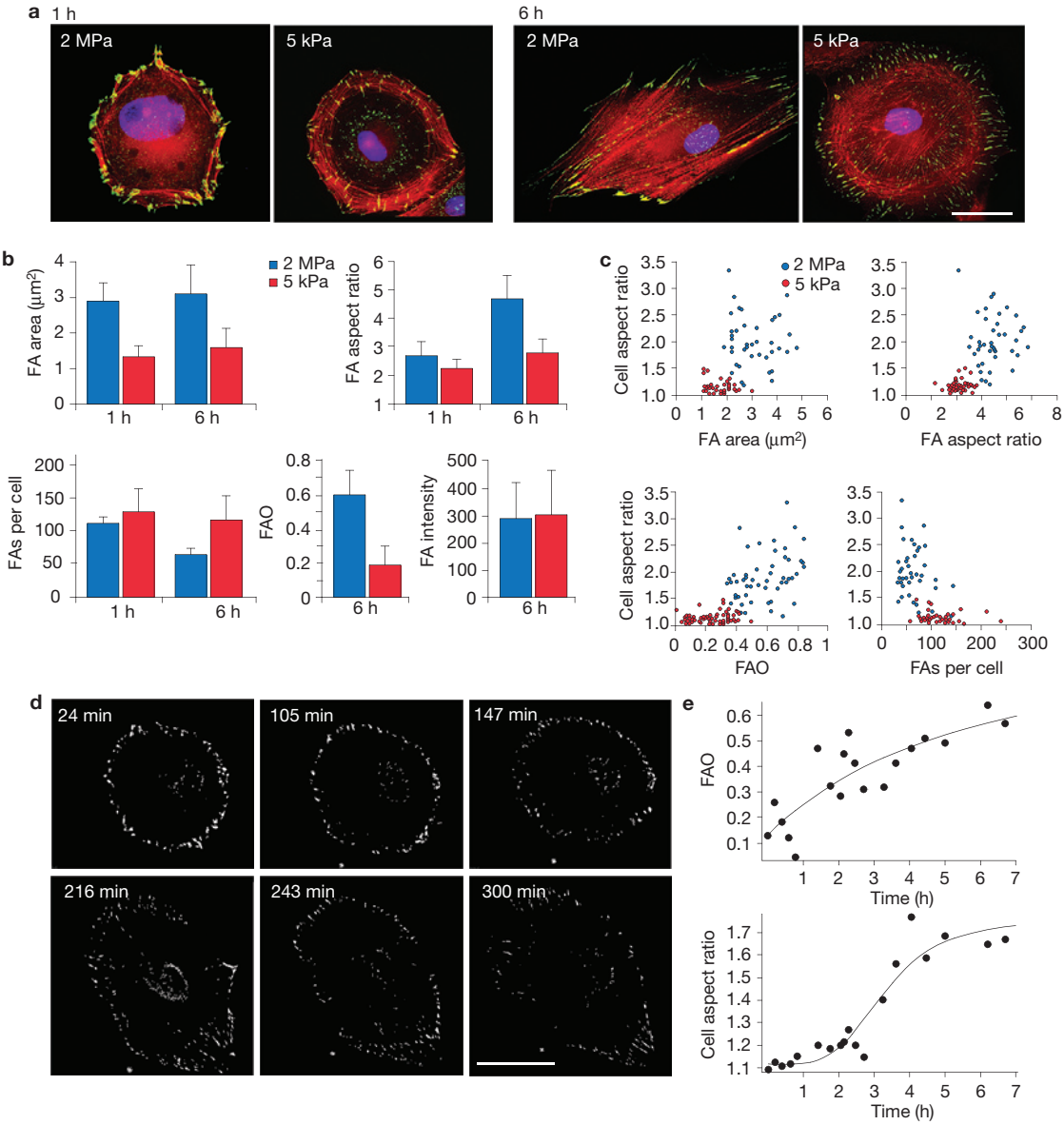

Figure 2 Characterization of focal adhesions in cells on stiff and compliant substrates. (**a**) HFF cells stably expressing paxillin–YFP (green) were plated on fibronectin-coated 2 MPa or 5 kPa PDMS substrates, and fixed at 1 and 6 h following seeding. Cells were stained with TRITC–phalloidin (red) and DAPI (blue). Scale bar, 30 μm. (**b**) Mean focal adhesion (FA) area, aspect ratio and number per cell at 1 and 6 h are shown in the first three panels. Indices of FAO and focal adhesion fluorescence intensity determined for cells fixed 6 h after seeding are shown in the last two panels. Bars represent average values, based on measurements of at least 40 cells per group. Error bars represent s.d. (**c**) Scatter plots showing correlations between focal adhesion parameters (area, aspect ratio, orientation and number of focal adhesions per cell) and cell elongation (aspect ratio), 6 h after cells were plated on 2 MPa (blue) and 5 kPa (red) substrates. Each dot within the plots corresponds to an individual cell: 40 cells were analysed for each type of substrate. (**d**) FA orientation (FAO) precedes cell elongation. HFF cells stably expressing paxillin–YFP were plated on fibronectin-coated glass coverslips. Recording of time-lapse movies started 30 min after plating, and lasted for about 7 h. Analysis of one representative cell, out of 14 cells with analogous behaviour, is presented. Frames taken from Supplementary Movie S3 were filtered and segmented to highlight the orientation of peripheral focal adhesions. Scale bar, 40 μm. (**e**) Indices of FAO (top) and cell aspect ratio (bottom) measured for the cell shown in Supplementary Movie S3. The solid lines represent the four-parameter logistic regression.

that did not polarize on either substrate (that is, the first group), the FAO index was consistently low (Fig. 4a) and focal adhesion number was relatively high (Supplementary Fig. S3). Cells that polarized on both rigid and compliant substrates (the second group) exhibited high levels of FAO (Fig. 4a) and low focal adhesion numbers per cell (Supplementary Fig. S3). In cells from the third group, the FAO values on the rigid substrate exceeded those exhibited by control cells (Fig. 4a). Moreover, unlike control and most other knockdowns, this group demonstrated a pronounced decrease in total focal adhesion area on the compliant substrate, compared with the rigid one (Supplementary Fig. S3). Thus, FAO and total focal adhesion area together seem to specify the type of polarization behaviour that cells exhibit.

The relationship between morphological features of individual focal adhesions (for example, size and aspect ratio) and cell polarization was more complex. Some knockdown cells that lost sensitivity to substrate rigidity at the polarization level still demonstrated a focal adhesion

Table 1 Cell polarization parameters in control and selected PTK-knockdown cells.

	Cell aspect ratio		Percentage of cells with long stress fibres		Percentage of cells with long stable edges		Cell area ($\mu m^2 \times 10^3$)	
	2 MPa	5 kPa	2 MPa	5 kPa	2 MPa	5 kPa	2 MPa	5 kPa
Control	2.2±0.06	1.5±0.04	77±4	24±4	78±4	50±5	4.1±0.19	4.5±0.15
CSFR1	1.3±0.03	1.3±0.03	23±4	14±4	22±5	19±4	6.2±0.58	5.5±0.38
ERBB4	1.5±0.06	1.4±0.05	41±5	25±4	43±5	32±5	6.1±0.41	5.7±0.39
CSK	1.5±0.04	1.3±0.02	54±5	34±5	45±5	39±5	4.2±0.20	5.7±0.37
FER	1.5±0.05	1.3±0.03	37±5	11±3	34±5	19±4	6.3±0.51	5.7±0.37
TYRO3	1.6±0.05	1.6±0.09	44±7	16±5	53±5	35±5	3.4±0.29	4.5±0.52
FGFR4	1.8±0.10	1.7±0.08	61±7	34±6	61±5	44±5	3.5±0.33	3.7±0.38
ROR2	2.2±0.07	1.9±0.11	65±4	58±5	84±4	66±5	5.0±0.31	6.0±0.50
PTK9	2.0±0.10	1.8±0.10	81±5	52±7	63±5	44±5	6.1±0.34	4.7±0.38
AXL	2.0±0.09	2.1±0.20	74±6	47±7	70±5	63±5	4.1±0.37	3.7±0.34
KDR	2.1±0.05	2.0±0.08	79±4	68±5	87±3	69±5	4.4±0.16	4.6±0.20
JAK1	2.1±0.07	1.9±0.07	85±4	52±5	79±4	62±5	3.8±0.13	5.1±0.30
FLT4	2.2±0.13	2.1±0.22	58±7	25±6	67±5	47±5	2.4±0.18	2.3±0.23
ERBB3	2.3±0.08	2.0±0.06	78±4	61±5	86±4	62±5	3.8±0.15	3.1±0.13
LTK	2.4±0.13	2.2±0.16	76±6	45±7	85±4	66±5	3.6±0.27	3.6±0.40
DDR2	4.5±0.08	2.1±0.06	80±4	35±5	87±3	67±5	3.9±0.18	5.1±0.25
MET	2.1±0.12	1.3±0.04	85±5	12±5	79±4	16±4	4.5±0.51	4.1±0.47
NTRK3	2.3±0.13	1.4±0.08	91±4	8±4	81±4	14±3	4.1±0.35	3.9±0.38
PTK2B	2.6±0.10	1.5±0.09	94±3	15±5	96±2	25±4	3.2±0.24	3.7±0.34

For each cell type (control and 18 selected and validated knockdowns) attached to rigid (2 MPa) and compliant (5 kPa) substrates, the average values (mean ± s.e.m.) of cell aspect ratio, percentage of cells with long stress fibres, percentage of cells with long stable edges and cell projected area are shown. For each cell type, 50–200 cells were measured. The selected knockdowns differ from control cells in aspect ratio or (and) in other polarization parameters. The knockdowns are sorted into three groups: cells that demonstrated low polarization on rigid and compliant substrates, cells that were highly polarized on both types of substrate, and cells that demonstrated greater differences in polarization between rigid and compliant substrates compared with normal cells. See also Supplementary Table S1.

rigidity response. In particular, members of the first group, FLT3 and EBB4, as well as members of the second group, FLT4, KDR, LTK, DDR2 and especially ERBB3, still formed focal adhesions of a larger size on the rigid substrate than on the compliant one (Fig. 4b,c). Even these knockdowns, however, demonstrated equal focal adhesion aspect ratios on both types of substrate (Fig. 4b,c).

Notably, in the other knockdown cell types, changes in focal adhesions strongly correlated with changes in cell polarization behaviour. Three knockdown cell types (CSF1R, CSK and FER) exhibited very small focal adhesions with low aspect ratios on both stiff and compliant substrates (Fig. 4b), and entirely lost their ability to polarize. Six knockdown cell types (TYRO3, PTK9, ROR2, FGFR4, AXL and JAK1) that exhibited focal adhesions of equal size and aspect ratio on both types of substrate polarized well in each instance (Fig. 4b,c). Finally, knockdown cells in the third group (NRTK2, NRTK3, MET and PTK2B) exhibiting higher differential polarization responses to compliant and rigid substrates, compared with control cells, demonstrated more pronounced differences in focal adhesion size on both types of substrate (Fig. 4b,c).

Measurements of the traction forces developed by cells on substrates with different rigidities enabled us to further dissect the alterations produced by knockdowns of diverse PTKs in the cellular response to substrate rigidity. We used 'net contractile moment', as defined previously[14], as a measure of overall cellular contractility. In agreement with previous studies addressing cell contractile response to substrate rigidity[15–17], we found that the net contractile moment of control cells was significantly lower on the 4 kPa substrate, compared with that on the 26 kPa substrate (Fig. 4c).

The responses of PTK-knockdown cells were diverse (Fig. 4c). In particular, TYRO3, FGFR4 and ERBB3 knockdowns showed high net contractile moments (close to that of control cells on the 26 kPa substrate) on both types of substrate, a finding consistent with the equal size (or equal aspect ratio) of the focal adhesions of these knockdowns on the rigid and compliant substrates. Surprisingly, however, several types of knockdown preserved the ability of normal cells to distinguish between substrates of varying rigidities, by developing traction forces of different magnitude. These included cell types such as CSK, FER and ERBB4 that do not polarize on any substrate type and form equally small focal adhesions, and cells such as ROR2 and AXL that polarize perfectly on both types of substrate and form relatively large and elongated focal adhesions in both instances (Fig. 4c). Obviously, in such knockdowns, focal adhesion formation is uncoupled from the traction force response to substrate rigidity.

DISCUSSION

This study addresses the molecular mechanisms underlying two basic properties of cultured fibroblasts: their ability to distinguish between extracellular matrices with varying degrees of stiffness, and their ability to acquire a polarized morphology following interaction with an appropriate substrate. Our findings demonstrate that these cellular characteristics are tightly interrelated: namely, the polarization of these cells requires a relatively rigid matrix, and does not occur on compliant substrates (in the 5 kPa range). Moreover, the mechanosensing machinery of focal adhesions seems to play an important role in regulating the rigidity-dependent cell polarization process.

Several lines of evidence indicate that surface rigidity sensing is mediated by integrin adhesions such as focal adhesions. These include the demonstration that focal adhesions are force-transducing, mechanosensory complexes, and their ability to grow in response to pulling forces requires attachment to an integrin-adhesive matrix[2,5,18–21]. In line with these findings, we demonstrated that the average size of focal adhesions on a fibronectin-coated 5 kPa PDMS substrate was about twofold smaller than those formed on rigid substrates (2 MPa) of the same type. These results are in agreement with other studies of focal adhesion

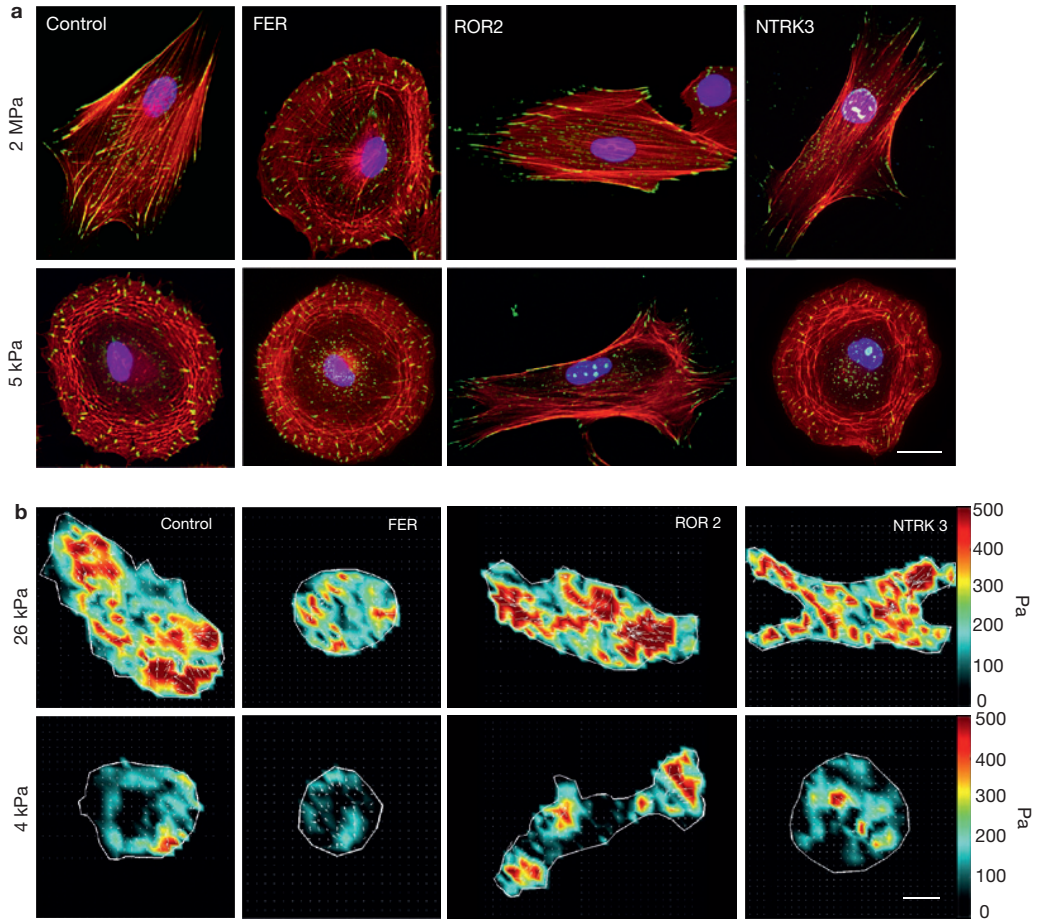

Figure 3 Examples of candidate knockdowns obtained from the siRNA screen. (**a**) Staining for actin (red), paxillin–YFP (green) and DAPI (blue) in control cells (left column) and cells with different PTK knockdowns. Scale bar, 25 μm. Cells with FER knockdown demonstrate a low level of polarization on rigid and compliant substrates; similar behaviour was observed in CSF1R, CSK, ERBB4 and FLT3 knockdowns. Cells with ROR2 knockdown were highly elongated on both types of substrate; such behaviour also typified 10 other knockdowns (AXL, JAK1, PTK9, ERBB3, FGFR4, FLT4, LTK, KDR, TYRO3 and DDR2). NTRK3-knockdown cells demonstrated greater differences in elongation between rigid and compliant substrates, compared with normal cells; similar behaviour was seen in NTRK2, MET and PTK2B knockdowns. (**b**) Traction force maps of control cells, and cells with selected PTK knockdowns, on 26 kPa or 4 kPa PAA gels. Scale bar, 25 μm. Traction fields were computed from the displacement of two fluorescence images of the microbeads, before and following cell removal by trypsin treatment. White arrows show the relative magnitude and direction of the displacement field of the tractions. Colours show the magnitude of the traction vectors in pascal units (see colour-coded bar).

formation on PDMS substrates with similar stiffness ranges[22]. We also found that focal adhesions formed on compliant substrates were considerably more mobile than those formed on rigid substrates.

Remarkably, examination of the polarization process on rigid surfaces by video microscopy revealed that cell elongation is often preceded by focal adhesion alignment in the direction of the future elongation axis. These observations are consistent with the idea that symmetry breaking leading to cell polarization is driven by the transition of focal adhesions from a radial distribution to an axial one, most likely due to stabilization of those sharing a similar orientation (those focal adhesions that are associated with parallel stress fibres), and the destabilization of the others. Our results show that such a process can occur only on a rigid substrate, and therefore depends on the mechanosensitivity of the focal-adhesion/stress-fibre system.

Tyrosine-kinase-driven signalling pathways seem to regulate many aspects of adhesion-mediated cellular morphogenesis; in particular, the cell's ability to respond to mechanical stimuli[12]. To elucidate the relationship between focal-adhesion/stress-fibre mechanosensitivity and cell polarization, we perturbed most of these potentially relevant signalling pathways by siRNA knockdown of 85 PTKs (ref. 9). By selecting the knockdown cells that significantly differed from controls (HFF) in their ability to polarize on substrates of varying degrees of stiffness, we identified 20 genes that are potentially involved in rigidity-dependent cell polarization. Examination of the ability of these knockdown cells to form focal adhesions on substrates with varying rigidities, together with estimations of the traction forces generated by these cells, provided insights into the molecular mechanisms underlying focal-adhesion/stress-fibre mechanosensitivity, as well as rigidity-dependent cell polarization.

Strikingly, altered polarization behaviour in most selected knockdown cell types (12 of 20) was accompanied by pronounced alterations in their focal adhesion response to substrate rigidity. Thus, these 12 genes may affect cell polarization through regulation of focal adhesion formation and response to substrate rigidity.

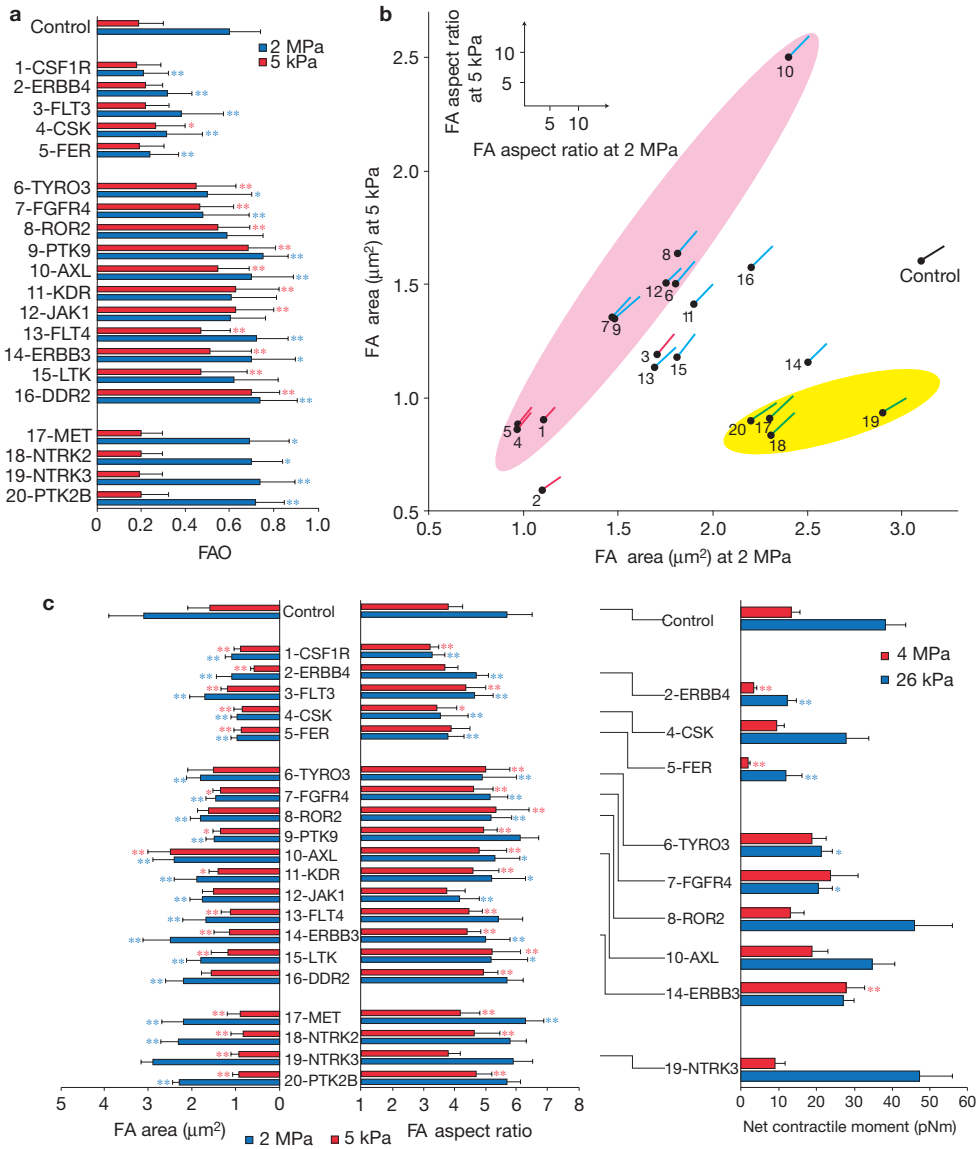

Figure 4 Morphological focal adhesion characteristics and net contractile moments in PTK-knockdown cells with altered rigidity-dependent polarization. (**a**) The values of average FAO ± s.d. for control cells, and knockdowns on rigid (2 MPa) and compliant (5 kPa) substrates. (**b**) Each cell type is represented by a point plotted in a coordinate system, in which the *x* and *y* axes correspond to average focal adhesion (FA) area on the rigid (2 MPa) and compliant (5 kPa) substrates, respectively. Focal adhesion aspect ratio values for these knockdowns are represented by the vectors radiating out from the corresponding points. Projections of these vectors onto horizontal and vertical axes (shown in the inset) correspond to the average focal adhesion aspect ratio values for the corresponding cells. The types of cell polarization behaviour (see text) are colour-coded: the first group (1–5) is shown in red, the second group (6–16) is shown in blue, and the third group (17–20) is shown in green. Highlighted are the knockdowns whose polarization behaviour strongly correlated with the focal adhesion response to substrate rigidity. Knockdowns that exhibited no difference in polarization behaviour on rigid and compliant substrates, and formed focal adhesions of the same size and aspect ratio, are delineated by a light pink ellipsis. Knockdowns that distinguished between rigid and compliant substrates more effectively than control cells in terms of polarization, and demonstrated a greater difference between focal adhesion size on rigid and compliant substrates, are delineated by a yellow ellipsis. (**c**) Values of focal adhesion area (left) and aspect ratio (middle; mean ± s.d.) on rigid and compliant substrates. Right, the net contractile moments (mean ± s.e.m.) of control cells and 9 selected knockdowns measured on PAA substrates with Young's moduli of 26 kPa (blue) and 4 kPa (red). The sample size for the measurements of focal adhesion parameters was 20 or 40 cells (see Methods) and for the net contractile moment, it was 10–24 cells of each type. Parameters of knockdown cells that significantly differ from the corresponding parameters of control cells at the *P*-value levels $P<0.05$ and $P<0.01$ are denoted by one and two asterisks, respectively.

Measurements of cell traction forces enabled us to dissect the regulatory roles of the corresponding genes. In several cases (ERBB3, TYRO3 and FGFR4), the formation of focal adhesions of similar size or aspect ratio on rigid and compliant substrates was accompanied by the generation of similar traction forces. However, other knockdowns, while forming focal adhesions of similar size on rigid and compliant substrates (CSK and FER — small; ROR2 and AXL — large), still clearly demonstrated a decrease in traction force on the compliant substrate. Thus, our experiments revealed a group of genes whose knockdown uncouples focal adhesion size from the strength of the traction forces

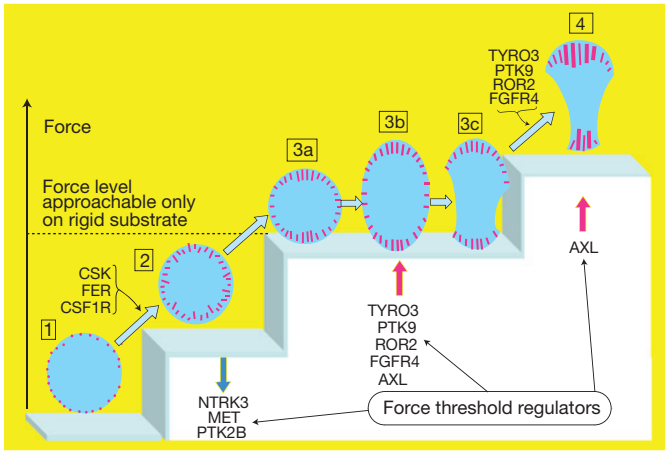

Figure 5 Focal-adhesion-guided cell polarization, and its regulation by PTKs. A schematic illustration depicting changes in focal adhesion and cell shape, as cells spread and polarize. The stages of cell polarization are defined as follows. 1, Radially spread cells with dot-like, nascent focal adhesions at the periphery[29,30]. 2, Radially spread cells with moderately elongated, radially oriented focal adhesions (the crosslinking function of myosin IIA may drive such focal adhesion elongation[30]). 3a, Radially spread cells in which the array of elongated focal adhesions, oriented in parallel, determines the future axis of polarization (focal adhesions oriented in other directions are smaller in size). 3b, A transient stage, depicting cell elongation along the prevalent direction of FAO. 3c, Polarized cells with non-adherent stable edges forming elongated focal adhesions of moderate size, oriented in parallel. 4, Fully polarized cells with large focal adhesions at the leading and trailing edges, and well-developed stable edges. Transitions from stages 1 to 2, 2 to 3, and 3 to 4 may depend on the development of pulling forces applied to focal adhesions and inducing their growth. The threshold level of the forces is depicted by steps. Genes required for some of the transitions depicted, as well as genes putatively participating in the regulation of threshold levels, are indicated. The arrows denote the direction of regulation: threshold decrease (down) or threshold increase (up). Knockdown of CSF1R, CSK and FER blocks focal adhesion growth at the nascent adhesion stage (transition from stage 1 to 2); therefore, these genes are required for focal adhesion elongation and maturation, irrespective of substrate rigidity and traction force. Knockdown of NTRK3, PTK2B and MET causes this transition to be rigidity dependent. In control cells, these genes may decrease the force threshold required for focal adhesion growth. Transition from stage 2 to 3 in control cells occurs only on rigid substrates, whereas in TYRO3, PTK9, ROR2, JAK1, AXL and FGFR4 knockdowns, focal adhesions can readily grow on compliant substrates as well. Transition from stage 3 to 4 does not occur in cells in which TYRO3, PTK9, ROR2, JAK1 and FGFR4 expression is suppressed. AXL-knockdown cells roughly approach stage 4 on both rigid and compliant substrates; hence, AXL may set a force threshold required for the final development of mature focal adhesions.

applied to them. Interestingly, it was recently demonstrated that such uncoupling between forces and focal adhesion size can occur physiologically during focal adhesion evolution in a single control cell[23].

Taken together, these results indicate that focal adhesion development is controlled at two levels (see the schematic drawing in Supplementary Fig. S4). One level involves the control of force production in response to differences in rigidity, and the other involves the control of focal adhesion sensitivity to the applied force. Several recent experimental and theoretical studies indicate that differential force production on substrates with varying rigidities may be related to features of the contractile actomyosin system *per se*[24–27].

On the basis of the combined results obtained for control and knockdown cells, we herein propose a unifying scheme of polarity development in fibroblasts, shown in Fig. 5, and delineate the roles of genes controlling focal adhesion formation and mechanosensitivity in this process (see legend to Fig. 5). In summary, this study, based on monitoring the concerted progression of cell polarization, focal adhesion development and traction force generation in control cells, as well as in cells in which specific PTKs were knocked down, highlights the central role of mechanosensing in cell polarization. It also points to specific stages in cell polarization that are regulated by focal adhesion reorganization, and identifies genes that are involved in controlling these processes. Further studies will be needed to elucidate the detailed molecular mechanisms underlying the involvement of these genes in cell mechanosensory functions. □

METHODS

Methods and any associated references are available in the online version of the paper at http://www.nature.com/naturecellbiology

Note: Supplementary Information is available on the Nature Cell Biology website

ACKNOWLEDGEMENTS

The authors are grateful to B. Morgenstern for expert help in preparing this article for publication. This work was financially supported, in part, by the National Institutes of Health (NIH) Common Fund Nanomedicine Program (PN2 EY016586), the Israel Science Foundation, the Minerva Foundation, the Maurice Janin Fund and the De Benedetti Foundation-Cherasco. B.G. holds the Erwin Neter Professorial Chair in Cell and Tumor Biology. A.D.B. holds the Joseph Moss Professorial Chair in Biomedical Research.

AUTHOR CONTRIBUTIONS

M.P-K. and A.L. participated in the design of the experiments, carried them out and analysed the data. R.K. and K.R. carried out the traction force microscopy analysis. A.M. and Z.K. contributed to the microscopy analysis, image processing and statistical analysis of the data. A.D.B. and B.G. supervised the project and participated in all of its aspects, including its design, data analysis and manuscript preparation.

COMPETING FINANCIAL INTERESTS

The authors declare no competing financial interests.

Published online at http://www.nature.com/naturecellbiology
Reprints and permissions information is available online at http://www.nature.com/reprints

1. Discher, D. E., Janmey, P. & Wang, Y. L. Tissue cells feel and respond to the stiffness of their substrate. *Science* **310,** 1139–1143 (2005).
2. Geiger, B., Spatz, J. P. & Bershadsky, A. D. Environmental sensing through focal adhesions. *Nat. Rev. Mol. Cell Biol.* **10,** 21–33 (2009).
3. Vogel, V. & Sheetz, M. Local force and geometry sensing regulate cell functions. *Nat. Rev. Mol. Cell Biol.* **7,** 265–275 (2006).
4. Guilak, F. *et al.* Control of stem cell fate by physical interactions with the extracellular matrix. *Cell Stem Cell* **5,** 17–26 (2009).
5. Janmey, P. A. & Miller, R. T. Mechanisms of mechanical signaling in development and disease. *J. Cell Sci.* **124,** 9–18 (2011).
6. Orr, A. W., Helmke, B. P., Blackman, B. R. & Schwartz, M. A. Mechanisms of mechanotransduction. *Dev. Cell* **10,** 11–20 (2006).
7. Vasiliev, J. M. Spreading of non-transformed and transformed cells. *Biochim. Biophys. Acta* **780,** 21–65 (1985).
8. Petrie, R. J., Doyle, A. D. & Yamada, K. M. Random versus directionally persistent cell migration. *Nat. Rev. Mol. Cell Biol.* **10,** 538–549 (2009).
9. Robinson, D. R., Wu, Y. M. & Lin, S. F. The protein tyrosine kinase family of the human genome. *Oncogene* **19,** 5548–5557 (2000).
10. Cramer, L. P. Forming the cell rear first: breaking cell symmetry to trigger directed cell migration. *Nat. Cell Biol.* **12,** 628–632 (2010).
11. Brunton, V. G., MacPherson, I. R. & Frame, M. C. Cell adhesion receptors, tyrosine kinases and actin modulators: a complex three-way circuitry. *Biochim. Biophys. Acta* **1692,** 121–144 (2004).
12. Giannone, G. & Sheetz, M. P. Substrate rigidity and force define form through tyrosine phosphatase and kinase pathways. *Trends Cell Biol.* **16,** 213–223 (2006).
13. Sawada, Y. *et al.* Force sensing by mechanical extension of the Src family kinase substrate p130Cas. *Cell* **127,** 1015–1026 (2006).

14. Butler, J. P., Tolic-Norrelykke, I. M., Fabry, B. & Fredberg, J. J. Traction fields, moments, and strain energy that cells exert on their surroundings. *Am. J. Phys. Cell Phys.* **282,** C595–C605 (2002).
15. Mitrossilis, D. *et al*. Single-cell response to stiffness exhibits muscle-like behavior. *Proc. Natl Acad. Sci. USA* **106,** 18243–18248 (2009).
16. Saez, A. *et al*. Traction forces exerted by epithelial cell sheets. *J. Phys. Condens. Matter* **22,** 194119 (2010).
17. Saez, A., Buguin, A., Silberzan, P. & Ladoux, B. Is the mechanical activity of epithelial cells controlled by deformations or forces? *Biophys. J.* **89,** L52–L54 (2005).
18. Bershadsky, A. D., Balaban, N. Q. & Geiger, B. Adhesion-dependent cell mechanosensitivity. *Annu. Rev. Cell Dev. Biol.* **19,** 677–695 (2003).
19. Puklin-Faucher, E. & Sheetz, M. P. The mechanical integrin cycle. *J. Cell Sci.* **122,** 179–186 (2009).
20. Schwartz, M. A. & DeSimone, D. W. Cell adhesion receptors in mechanotransduction. *Curr. Opin. Cell Biol.* **20,** 551–556 (2008).
21. Hoffman, B. D., Grashoff, C. & Schwartz, M. A. Dynamic molecular processes mediate cellular mechanotransduction. *Nature* **475,** 316–323 (2011).
22. Goffin, J. M. *et al*. Focal adhesion size controls tension-dependent recruitment of alpha-smooth muscle actin to stress fibers. *J. Cell Biol.* **172,** 259–268 (2006).
23. Stricker, J., Aratyn-Schaus, Y., Oakes, P. W. & Gardel, M. L. Spatiotemporal constraints on the force-dependent growth of focal adhesions. *Biophys. J.* **100,** 2883–2893 (2011).
24. Fouchard, J., Mitrossilis, D. & Asnacios, A. Acto-myosin based response to stiffness and rigidity sensing. *Cell. Adh. Migr.* **5,** 16–19 (2011).
25. Mitrossilis, D. *et al*. Real-time single-cell response to stiffness. *Proc. Natl Acad. Sci. USA* **107,** 16518–16523 (2010).
26. Walcott, S. & Sun, S. X. A mechanical model of actin stress fiber formation and substrate elasticity sensing in adherent cells. *Proc. Natl Acad. Sci. USA* **107,** 7757–7762 (2010).
27. Webster, K. D., Crow, A. & Fletcher, D. A. An AFM-based stiffness clamp for dynamic control of rigidity. *PLoS One* **6,** e17807 (2011).
28. Montgomery, D. C. & Runger, G. C. *Applied Statistics and Probability for Engineers* 2nd edn (John Wiley, 1999).
29. Alexandrova, A. Y. *et al*. Comparative dynamics of retrograde actin flow and focal adhesions: formation of nascent adhesions triggers transition from fast to slow flow. *PLoS One* **3,** e3234 (2008).
30. Choi, C. K. *et al*. Actin and α-actinin orchestrate the assembly and maturation of nascent adhesions in a myosin II motor-independent manner. *Nat. Cell Biol.* **10,** 1039–1050 (2008).

DOI: 10.1038/ncb2370

METHODS

Cells. HFFs, retrovirally infected with yellow fluorescent protein (YFP)-tagged human paxillin in pBabe vector[31] were cultured in Dulbecco's modified Eagle's medium supplemented with 10% fetal calf serum, 2 mM glutamine and antibiotics (penicillin and streptomycin). Tissue culture medium, antibiotics, trypsin/EDTA solution and glutamine (Gibco) were obtained from Rhenium, and fetal calf serum was obtained from Biological Industries.

Chemicals and reagents. Nocodazole (methyl[5-(2-thienylcarbonyl)-1H-benzimidazol-1-yl]-carbamate), taxol (paclitaxel), poly-L-lysine, TRITC-labelled phalloidin, DAPI and tissue-culture-grade fibronectin were purchased from Sigma-Aldrich. Blebbistatin was purchased from Calbiochem.

Preparation of substrates of varying rigidities. PDMS substrates of varying rigidities were prepared using a Sylgard 184 silicone elastomer kit (Dow Corning). The silicone elastomer component was mixed with the curing agent, degassed and spin-coated at 2,000 r.p.m. for 2 min with a Spin Processor WS-650MZ-23NPP/LITE (Laurell Technologies) on #1 microscopy coverslips (Electron Microscopy Science) to obtain a 35 ± 5 μm-thick PDMS layer. Subsequently, crosslinking of the elastomer was carried out at 70 °C for 4 h. Polymerized slabs of PDMS were used for bulk measurements of Young's moduli, using an Instron universal testing machine (Instron). Elastomer to curing agent ratio: 10:1, 25:1, 50:1 and 75:1 corresponded to Young's moduli 2 MPa, 700 kPa, 20 kPa and 5 kPa, respectively. Coverslips with a layer of PDMS were functionalized with 20 μg ml^{-1} fibronectin overnight at 4 °C. Before cell plating, plates were washed with PBS and growth medium. Uniformity and density of fibronectin coating was tested microscopically, using Alexa 405-labelled fibronectin (provided by F. Anderegg, ETH, Zürich, Switzerland). Fibronectin densities on PDMS substrates with different Young's moduli were identical. PAA substrates with Young's moduli of 150, 30, 26 and 4 kPa were prepared and coated with 20 μg ml^{-1} fibronectin, as previously described[32].

Fluorescence microscopy. For live-cell imaging, an Olympus IX71 inverted fluorescence microscope equipped with an Olympus Plan ApoN ×40/0.75 NA or ×20/0.7 NA objectives, and a Box & Temperature & CO_2 control unit (Life Imaging Services) was used. Time-lapse filming was carried out at 2–5-min intervals. For examination of fixed specimens, ×60/1.42 NA or 20×/0.7 NA objectives were used. Image acquisition was carried out using a CoolSNAP HQ CCD camera (Photometrics), controlled by a DeltaVision system (Applied Precision).

Traction force microscopy. As cell-driven deformations of the very rigid substrate (2 MPa) are undetectable, we compared traction force development on the fibronectin-coated PAA substrates with rigidities of 4 and 26 kPa, respectively. We found that control cells did respond to such rigidity differences, consistent with our results for cell aspect ratios on PAA gels with rigidities of 4 and 30 kPa (Fig. 1). Cell traction was determined using constrained Fourier transform traction microscopy[32]. Briefly, the displacement field was computed by comparing fluorescent microbead images obtained during the experiment with the reference image obtained at the end of the experiment, following the detachment of cells from the substrate by trypsinization. From the displacement field, we calculated the traction field, as described in ref. 32. The contractile moment (T) was calculated by summing the diagonal components of the shear moment matrix (M) in its principal form (M^{rot}).

$$T = \mathrm{trace}\,(M^{\mathrm{rot}}) = M_{xx}^{\mathrm{rot}} + M_{yy}^{\mathrm{rot}}$$

where M_{xx}^{rot} and M_{yy}^{rot} represent the total contribution of cell–substrate contractions in the x and y directions, respectively[32].

Image analysis. The projected area and best-fit ellipse aspect ratio of TRITC–phalloidin stained cells were calculated using ImageJ software. For analysis of focal adhesion characteristics, the images of paxillin–YFP-expressing cells were segmented using the Watershed algorithm[33,34] and analysed using the Priism software package. Areas of individual focal adhesions, focal adhesion aspect ratio, number of focal adhesions per cell, intensity of paxillin–YFP fluorescence in focal adhesions and FAO in the cell were determined. The FAO is defined as $(P_x{}^2 + P_y{}^2)^{1/2}$, where P_x and P_y are the average values of $\cos(2\theta)$ and $\sin(2\theta)$, respectively, and θ is an angle between the focal adhesion and the x axis; an average is taken for all focal adhesions in the cell, and weighted by focal adhesion area. This index ranges from 1 (all focal adhesions are oriented in parallel) to 0 (focal adhesions are oriented randomly). Focal adhesion dynamics was assessed by ratio imaging of time-lapse movies, as previously described[31].

siRNA library. The Human ON-TARGETplus SMARTpool Tyrosine Kinase siRNA Library (Dharmacon RNAi Technologies) was used for the primary screen (see accession numbers in Supplementary Table SI). To validate specific hits, we used four individual siRNA sequences corresponding to the knockdown candidates selected. When two or more sequences induced the same effect as that observed by the SMARTpool in the primary screen, the candidate gene was considered to be validated (see Supplementary Table S2). For both primary screen and validation, the siRNA concentrations were 50 nM.

Note that the PTK9 gene from the library selected and validated by our screen does not belong to the tyrosine kinase category, as previously suggested[35], but is an actin-monomer-binding protein[36].

Screening protocol. HFF cells expressing paxillin–YFP were plated on 96-well plates (2,000 cells per well) and transfected with Dharmacon reagents 24 h later, according to the manufacturer's instructions. Transfections were carried out in two independent 96-well plates. Each plate contained two wells with siCONTROL TOX as an internal transfection efficiency control. In the plates selected for the screen, the transfection rates were 90%. At 72 h after transfection, cells were trypsinized and replated onto 96-well plates (TeleChem International) with bottoms made of glass coverslips coated with a 35 ± 5 μm-thick layer of 2 MPa or 5 kPa PDMS. The coverslips were coated with fibronectin, before mounting. At 6 h following plating, cells were fixed with 3% paraformaldehyde in phosphate-buffered saline (PBS) containing 0.25% Triton X-100 for 20 min, washed three times with PBS, and stained with DAPI and TRITC–phalloidin. The plates were then disassembled, and the bottom coverslips were mounted on the slides using Elvanol (Mowiol 4-88, Hoechst), and analysed using fluorescence microscopy.

Selection of candidate knockdowns and statistical analysis. The screening procedure consisted of three steps. In the first step, the parameters characterizing cell morphology (Supplementary Fig. S1 and Table S1), including average aspect ratios (AR), percentage of cells with long stress fibres, percentage of cells with long stable edges and average cell projected area, of control and 85 different knockdown cells were measured on rigid (r) and compliant (c) substrates, in at least 20 cells in each case. Knockdowns were then sorted according to the difference in their aspect ratio on rigid and compliant substrates, using a parameter $\Delta_{\mathrm{AR}} = (AR_{\mathrm{r}} - AR_{\mathrm{c}})/AR_{\mathrm{r}}$. Of the sorted list, 30 knockdowns (10 with the highest and 20 with the lowest Δ_{AR} values) were selected for further study. These knockdowns showed either markedly enhanced or markedly decreased rigidity sensing, compared with control cells.

For the second step, the average aspect ratio, percentage of cells with long stress fibres, percentage of cells with long stable edges and cell projected area values for 30 selected knockdowns were measured, in at least 50 cells per knockdown. At the end of this screening step, 20 knockdowns characterized either by the highest or lowest values of Δ_{AR} (no. 1–15 and 81–85 in Supplementary Table S1) were chosen for the measurements of focal adhesions and traction forces. Among these 20 knockdowns, 18 passed the validation (Table 1). For all of these knockdowns, the values of at least one morphological parameter on at least one type of substrate (rigid or compliant) significantly differed from corresponding values for the control cells ($P < 0.05$).

Estimation of the focal adhesion parameters (area, aspect ratio, number per cell and orientation) was carried out, first for at least 20 cells from the control culture, and each of the 20 selected knockdowns. The significance of the difference between average parameter values on the rigid and compliant substrates, as well as between the average values of corresponding parameters of knockdowns versus control cells, was calculated for each of the knockdowns, using a two-tailed Student t-test. To further improve the reliability of our data, we then selected those knockdowns for which a non-significant difference of at least one focal adhesion parameter from controls, or between rigid and compliant substrates, could potentially become significant ($P < 0.05$) if the number of measured cells was increased. To this end, the P values were recalculated for a twofold higher number of cells, assuming that the mean and standard deviation values remained the same. Such recalculation led to altered significance in 8 or the 20 knockdowns (CSF1R, FER, FGFR4, AXL, KDR, DDR2, NTRK3 and PTK2B). To confirm our previous results, we also chose two knockdowns (ERBB3 and ERBB4) that demonstrated very clear-cut, quantitative results when the 20 cells were measured. For each of these 10 cases, as well as for control cells, we carried out the measurements using a twofold-increased number of the cells (40).

31. Winograd-Katz, S. E., Itzkovitz, S., Kam, Z. & Geiger, B. Multiparametric analysis of focal adhesion formation by RNAi-mediated gene knockdown. *J. Cell Biol.* **186,** 423–436 (2009).
32. Butler, J. P., Tolic-Norrelykke, I. M., Fabry, B. & Fredberg, J. J. Traction fields, moments, and strain energy that cells exert on their surroundings. *Am. J. Phys. Cell Phys.* **282,** C595–C605 (2002).
33. Kam, Z., Zamir, E. & Geiger, B. Probing molecular processes in live cells by quantitative multidimensional microscopy. *Trends Cell Biol.* **11,** 329–334 (2001).
34. Zamir, E. *et al.* Molecular diversity of cell-matrix adhesions. *J. Cell Sci.* **112 (Pt 11),** 1655–1669 (1999).
35. Beeler, J. F., LaRochelle, W. J., Chedid, M., Tronick, S. R. & Aaronson, S. A. Prokaryotic expression cloning of a novel human tyrosine kinase. *Mol. Cell Biol.* **14,** 982–988 (1994).
36. Vartiainen, M., Ojala, P. J., Auvinen, P., Peranen, J. & Lappalainen, P. Mouse A6/twinfilin is an actin monomer-binding protein that localizes to the regions of rapid actin dynamics. *Mol. Cell Biol.* **20,** 1772–1783 (2000).

nature cell biology

DOI: 10.1038/ncb2370

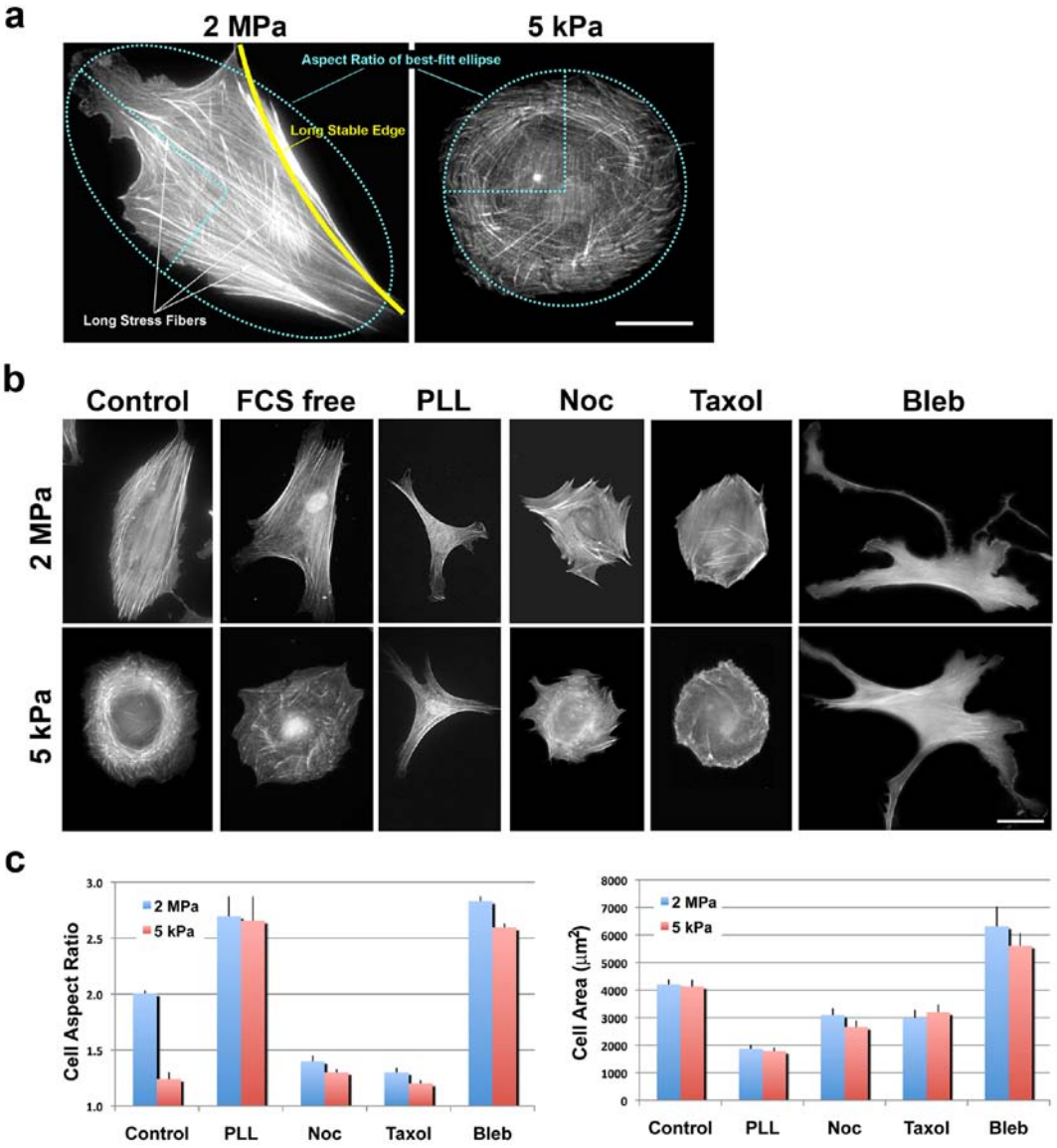

Figure S1 Factors affecting the ability of cells to polarize on rigid and compliant substrates. (a) Assessment of cell polarization. HFF cells fixed 6 h after plating on rigid (left) and compliant (right) FN-coated PDMS substrates were stained with TRITC-phalloidin to visualize F-actin. Scale bar: 25 μm. Three parameters were used to quantify cell polarization: (1) Cell aspect ratio (AR), the ratio of the long axis to the short axis of the best-fit ellipse; (2) Fraction of cells with long stress fibers (SF): The cell was seen as having long stress fibers when the length of at least one of them exceeded the radius of the cell's circumcircle (the smallest circle that completely contains the cell contour); (3) Fraction of cells with long stable edges (SE): the length of the "long" stable edge should exceed, in length, the radius of the cell's circumcircle [1]. (b) Effects of various treatments. HFF were plated on FN-coated 2 MPa or 5 kPa PDMS substrates in serum-containing ("control") or in serum-free ("FCS free") medium (2 left panels, respectively), or on 50 mg/ml poly-L-lysine (PLL)-coated substrates in serum-free medium. Cells plated on FN-coated substrates in serum-containing medium were treated with one of the following cytoskeleton-affecting drugs: 2.5 mM nocodazole (noc), 24 mM taxol, or 50 mM blebbistatin (bleb). In all cases, cells were fixed 6 hours after seeding, and stained with TRITC-phalloidin. Scale bar: 30 μm. (c) Graphs show the cell aspect ratio (left) and projected area (right). Error bars represent standard error of mean (SEM). At least 30 cells were measured for each type of cell treatment. Note that cells attached to the PDMS substrate in serum-free medium coated with PLL demonstrated uniform polarization behavior, irrespective of substrate rigidity. The cells lacked a system of parallel stress fibers and a polarized leading edge, which are crucial features of cell polarization. Cell treatment with nocodazole or taxol totally blocked elongation of HFF on both types of substrates. Cells treated with blebbistatin displayed a similar morphology on both rigid and compliant substrates, characterized by numerous arborized processes and a high aspect ratio, but failed to develop a polarized leading edge, nor did they form oriented stress fibers.

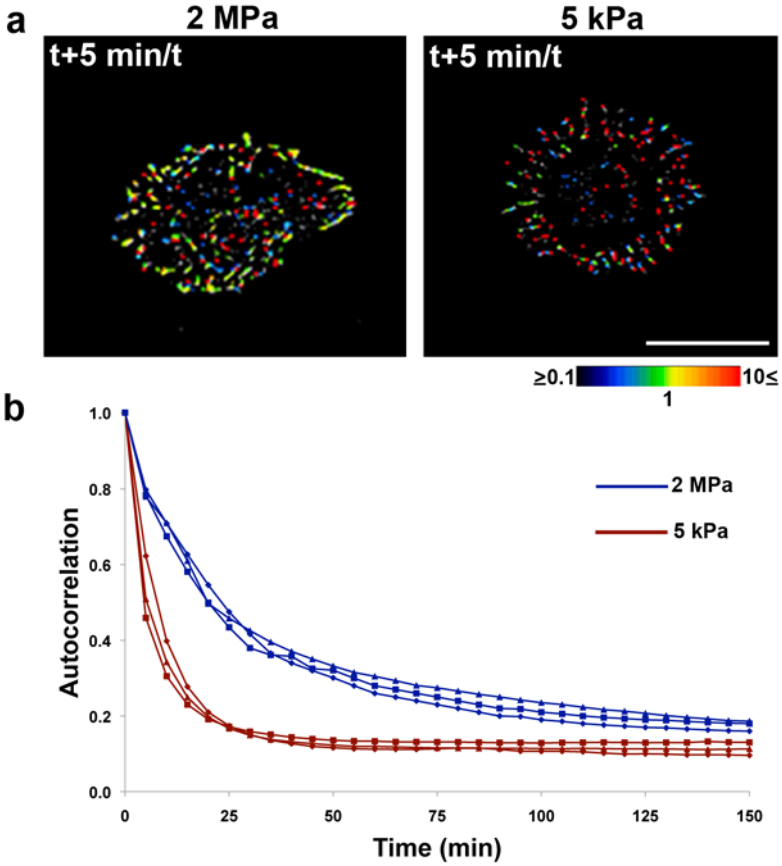

Figure S2 Focal adhesion dynamics on rigid and compliant substrates. (a) Temporal ratio images showing the difference between FA positions in two frames, taken 5 min apart, in YFP-paxillin-expressing cells plated on 2 MPa (left) and 5 kPa (right) FN-coated PDMS substrates. The ratio values are color-coded, such that FAs or their segments that appeared during this time are colored blue, those that disappeared are colored red, while those that remained unchanged are colored yellow. Scale bar: 40 mm. (b) Curves showing decay of the spatial correlation between FA images over time were calculated for cells growing on 2 MPa or 5 kPA substrates. Auto-correlation was calculated by comparing the adhesions at each time point, with those at time point zero. Pooled results from triplicate movies of cells spreading on each type of substrate are shown. The analyzed movie frames contained 2-7 individual cells. Note that the extracted decay time is faster on compliant (7.4±1.9 min) than on rigid substrates (24.8±1.9 min).

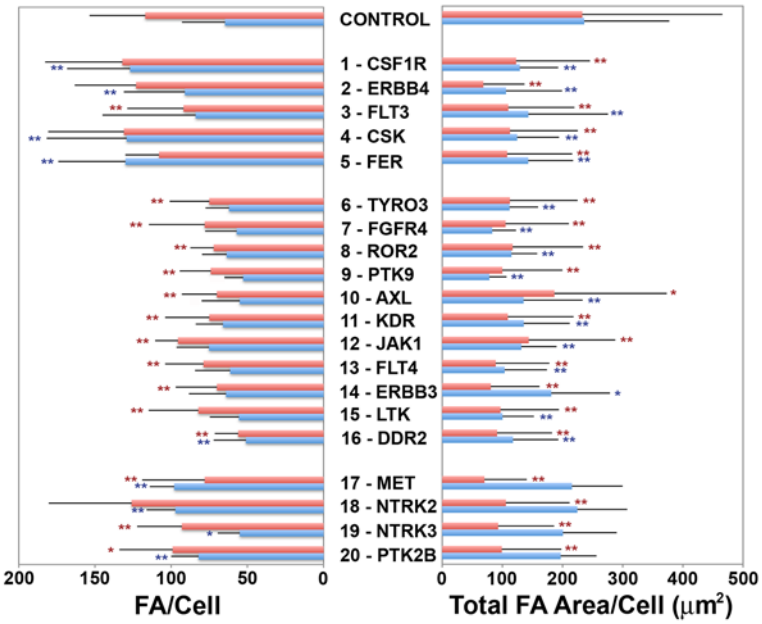

Figure S3 Focal adhesion numbers and total focal adhesion area per cell. The average number of FAs per cell (left column) and the values of total FA area per cell (right column) are shown for control cells, and three groups of knockdowns on rigid (blue bars) and compliant substrates (red bars). The average value of the total FA area per cell, was obtained by multiplying the average area of individual FAs per cell, by the average number of FAs per cell. Error bars represent standard deviations. Sample size for the measurements of FA parameters was 20 or 40 cells of each type (see Methods). For each parameter, statistically significant differences between knockdown and control ($p<0.05$ and $p<0.01$) are denoted by one or two asterisks, respectively.

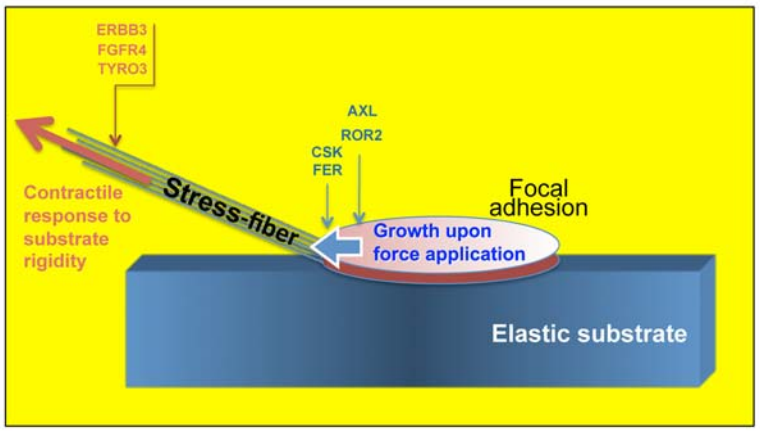

Figure S4 Differential regulation of cell mechanosensory response to substrate rigidity. A scheme depicting the complexity of the cell mechanosensory response to substrate rigidity. Knockdowns of all genes indicated here abolished the difference between the sizes (or at least the aspect ratios, in the case of ERBB3 knockdown) of focal adhesions formed on substrates with varying rigidities. Some of these knockdowns (ERBB3, FGFR4, and TYRO3) also abolished the difference between traction forces developed by the cells, while others (AXL, ROR2, and CSK) do not interfere with the development of stronger traction forces on the more rigid substrates. We hypothesize that ERBB3, FGFR4, and TYRO3 genes regulate the contractile response to substrate rigidity, while AXL and ROR2 establish the force threshold for the focal adhesion assembly. CSK is required for focal adhesion growth: when knocked down, the focal adhesions remain small, even if they experience strong contractile forces.

Supplementary tables

Table S1 Cell polarization parameters in control and PTK-knockdown cells.
For each cell type (control and 85 knockdowns) attached to rigid (r) and compliant (c) substrates, the average values of AR, SF, SE and cell projected area (A) are shown in subtables a-d, respectively. The normalized differences between the corresponding parameters on rigid and compliant substrates (DAR, DSF, DSE, DA) are shown in the right column of each subtable. For each type of parameter (a-d), knockdowns were sorted according to the ascending values of corresponding Ds. Among 15 knockdowns demonstrating the smallest DARs, we distinguished between those that elongated weakly (first group, highlighted in pink), and those that elongated strongly (second group, highlighted in blue), on both types of substrates. Four knockdowns demonstrating the greatest DARs were highlighted in green (third group). The DDR2-knockdown demonstrated unique behavior: On the one hand, its DAR was the highest among all the knockdowns; therefore, in a formal sense, it could be included in the third group. On the other hand, for this knockdown, AR on both types of substrate was much higher than in control cells, so that DDR2 knockdown cells could be regarded as being polarized on both types of substrates. In addition, the ability of these cells to form stable edges and oriented arrays of long stress fibers was similar on both rigid and compliant substrates. For these reasons, we included these cells within the second group of knockdowns (blue). All selected knockdowns were marked with corresponding colors.

Table S2 Validation of "SMARTpool" siRNAs
Effects of individual siRNA duplexes on the polarization behavior of transfected cells on rigid and compliant substrates were assessed. Listed are the sequences that induce the same phenotype as the SMARTpools. When two or more sequences induce the same effect as the one induced by the corresponding SMARTpool in the primary screen, the candidate gene is considered validated.

1. Prager-Khoutorsky, M. *et al.* Allicin inhibits cell polarization, migration and division via its direct effect on microtubules. *Cell Motil Cytoskeleton* **64**, 321-337 (2007).

Supplementary movie legends

Movie S1 Spreading of cells on stiff or compliant substrates
Fluorescence images of spreading cells on 2 MPa (left) or 5 kPa (right) substrates were recorded at 5 min intervals over a period of 10 hrs; the first image was taken 30 min after cells were plated. Note that on 2 MPa substrates, cells spread and, within 1-3 hours, become polarized and start to migrate; while on 5 kPa substrates, they retain a discoid shape. Display rate: 10 frames/sec.

Movie S2 Temporal ratio video of cell spreading on rigid or compliant substrates
The ratio images of HFF cells on 2 MPa (left) or 5 kPa substrates (right) taken in 5 min interval, are presented on a color spectrum scale, such that "new pixels" are blue, pixels that disappeared are red, and other pixels in FAs are represented by varying colors (orange-yellow-green), depending on the specific local intensity ratio. Yellow indicates identical intensities at the two time points. A representative frame from this video is shown in Fig. 3a. Display rate: 10 frames/sec.

Movie S3 Focal adhesion orientation precedes cell elongation
Images of YFP-tagged paxillin in a spreading cell were recorded at 3 min intervals over a period of 7 hours. Time-lapse movie started 30 min after plating. Display rate: 10 frames/sec. Note that apparent alignment of FAs in the direction of the future axis of cell elongation occurs, while the cell itself is still round.